Article

Correction of Field-Measured Wind Speed Affected by Deterministic Interference Factors

Jing Duan [1], Xingyu Chen [1], Zhuangning Xie [1,*] and Lele Zhang [1,2]

[1] State Key Laboratory of Subtropical Building Science, South China University of Technology, Guangzhou 510641, China; duanjingyuanyuan@163.com (J.D.); 201921008400@mail.scut.edu.cn (X.C.); zhanglele19891217@163.com (L.Z.)

[2] China Construction Second Engineering Bureau Co., Ltd., South China Company, Shenzhen 518048, China

* Correspondence: znxie@scut.edu.cn

Abstract: The observations of meteorological wind speed may be biased due to the influence of various distractions. Therefore, the original measured data should be corrected in a targeted manner. Wind tunnel tests (WTT) and computational fluid dynamics (CFD) numerical simulation methods are used to study the local wind environment characteristics of observation sites in Noi Ling Ding Island (NLDI) and Ping An International Financial Center (PAFC) in the Shenzhen area. The interference effects of NLDI and the building components and instruments in the hollow-layer atop PAFC on their corresponding anemometer measurement results were analyzed, and a quantitative description was provided with the wind speed influence coefficient (C_{VI}), which is the wind speed ratio in disturbed and undisturbed cases. Results show that the C_{VI} of WTT at the NLDI site is slightly higher than that of CFD, and the wind speed in the wind-sensitive direction is accelerated by 12% due to the influence of NLDI. The large pillars at the corner of PAFC have a considerable occlusion effect on the wind speed under the wind direction of 45°. An acceleration effect with C_{VI} of 1.163 is found in the dominant wind direction when instruments are absent atop the hollow-layer, whereas a sheltering effect is observed with the C_{VI} of 0.593 when instruments are present. These results are used to correct the recorded wind speed at the NLDI and PAFC sites during Super Typhoon Manghut with No. 201822, and then converted into the 10 min mean wind pressure value at 10 m height under the standard landform. The reference wind pressure values obtained are 0.526 and 0.505 kPa. The analogous conversion values achieve the purpose of mutual verification, and the effectiveness and reliability of the methodologies are presented.

Keywords: field measurement; distraction; wind speed correction; WTT; numerical simulation

1. Introduction

Meteorological wind speed information is the main data source for analyzing near-ground wind characteristics in the atmospheric boundary layer in the field of structural wind resistance. It plays an extremely important and decisive role in the reasonable estimation and accurate evaluation of structural wind load. The measured weather data are generally received from near-ground meteorological masts or wind measurement instruments installed on high-rise buildings. However, due to the impact of urbanization, the upstream and surrounding environments of the sites are far coarser than the open terrain stipulated in relevant specifications. Therefore, the measured results of wind speed are different from those on the open terrain and must be revised.

Field measurement, wind tunnel test (WTT), and computational fluid dynamics (CFD) numerical simulation are conventional research methods in structural wind engineering [1,2]. WTT can study the interaction between the model with a certain scale ratio and the simulated gas flow, and the numerical simulation can observe the gas flow globally at full scale and provide the entire flow field data. Furthermore, the combined application of the two methods can verify and replenish field measurement results. In the studies of local

wind environment, all the methods have effective applications, especially in describing the properties of the air flow movement of terrain or buildings.

To determine the influence of terrain on air flow, although definite calculation methods for terrain factors of 2D and symmetrical 3D terrain are available in many specifications, the air flow over complex terrain should be studied by means of field measurement, WTT, and numerical simulation. For example, the air flow affected by terrain in the Askervein hill in Scotland has been continuously studied in the past 30 years. First, Teunissen et al. [3] (1987) carried out a WTT of the hill at three different length scales, and they evaluated the effects of surface roughness, model scale, and measurement techniques on the mean wind speed and turbulence. The WTT results agreed well with the field measurements. With the development of numerical simulation theory and the maturity of technology, researchers improved the turbulence model [4–7] and simulated the air flow over the isolated Askervein hill by using the 3D nonlinear numerical model, the Reynolds-averaged Navier–Stokes (RANS) model, and the large eddy simulation (LES). The results show that the precision of the LES model is relatively higher, and the simulation effect of the windward side is better than that of the leeward side. For the acceleration effect, which is the concern of most structural designers, Flay et al. [8] (2019) discussed the wind speed ratio of nine measuring points at Belmont Hill in New Zealand through the WTT with a scale of 1:2000, full-scale numerical simulation, and field measurement. The results also show that the consistency between WTT and field measurement is better than that of CFD. Meanwhile, when these results are compared with the recommended values in AS/NZS1170.2 [9] (2011), the results calculated by the specifications are found to have significant deviations.

In addition, for some air flow problems related to building wind environment [10–13], such as comfort of pedestrian wind environment, wind effect of passage between buildings, and indoor air flow prediction wind cross ventilation, especially in exploring the variation patterns of wind speed, wind direction, wind pressure, eddy, and other parameters at local measured points, the combined application of multiple methodologies can solve the relevant problems relatively well. Iqbal et al. [14] investigated the influence of the wind incident angle and passage width on the wind flow characteristics at the re-entrant corners of cross-shaped high-rise buildings and the pedestrian-level wind comfort. They selected the standard *k-ε* turbulence model for RANS steady-state analysis in numerical simulation after considering the calculation cost and the accuracy balance. In addition, the normalized wind speed ratios at the re-entrant corners by the two methods were compared. The results show that the fluctuation of the WTT results is more evident. Jaminska et al. [15] simulated the air flow changes of two non-parallel walls (with an angle of 100°) atop the bell tower under divergent and converging wind directions by CFD, and then verified them with the field measurement results. The results also show that the effect of wind speed amplification or contraction observed in numerical simulation and full-scale measurement are consistent. James Lo L. et al. [16] proposed a combination of WTT and CFD to predict the indoor air flow of wind-induced cross ventilation and introduced the wind pressure test data of the WTT as the boundary condition into the CFD numerical simulation. Then, the steady-state and transient analysis were used to compare the mean flow rate and the instantaneous velocity, which were verified by the full-scale measurement results to assess the cross-ventilation potential of the building.

In general, the WTT uses wind speed sensors to measure air flow changes under the analog simulation air flow. However, it is often limited by the model scale ratio, the blockage ratio, and the wall Reynolds number. Nevertheless, compared with the dependence of the simulation precision and the computational parameters [17], such as the size of the computational model, the resolution of the computational grid, the inlet turbulent kinetic energy profile of the atmospheric boundary layer, the turbulence model, the order of the discretization schemes, and the iterative convergence criteria, the stable implementation conditions of the WTT increase result recognition.

Two stations with relatively stable surrounding environment, namely, Noi Ling Ding Island (NLDI) and hollow-layer Ping An International Financial Center (PAFC), are consid-

ered the research objects to obtain the accurate wind speed in the Shenzhen area during typhoon landfall. The WTT and CFD numerical simulation were conducted to study the local wind environment characteristics of the sites. The influence of NLDI and structural components and instruments in the hollow-layer of PAFC on the measured results of the corresponding anemometers was analyzed, and the correlation between the wind speed influence coefficient (C_{VI}) and wind direction was established. The measured meteorological wind speeds were corrected, and the corresponding maximum reference wind pressures were converted based on the revised results.

2. Site Overviews and Wind Conditions

NLDI is an isolated island located in the Pearl River estuary area, which is in the southwest of Shenzhen, with the highest elevation of approximately 300 m. The location of the station is the south end of the island (113.8° E, 22.42° N) and the surrounding landform is an open Pearl River water and low island vegetation. Hong Kong Tuen Mun District is 9 km to the east of the station, Hong Kong Airport (HKIA) is 13 km away to the southeast, and Shenzhen Nanshan District is 9 km away to the northeast (Figure 1). Theoretically, the interference of the surrounding environment on the measured wind speed is relatively minimal. However, as the wind mast is located at the end of the island and only 65 m above sea level, the measured wind speed may be affected by the island itself.
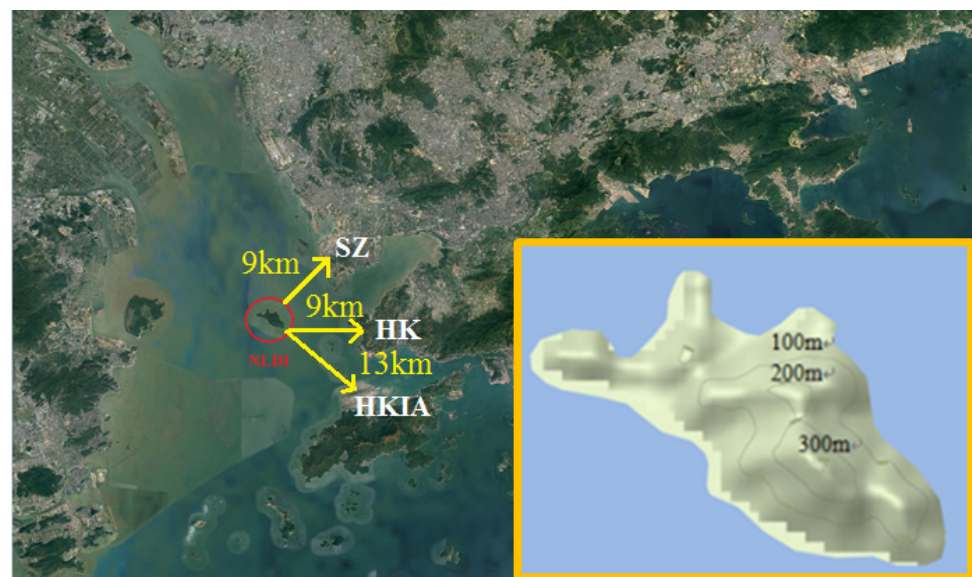

Figure 1. Landscape around NLDI.

PAFC is located in Futian district with the height of 592.5 m, and an 8 m high hollow-layer is found at the height of 576.0 m (Figure 2). The hollow-layer plane is an inclined four degree slope one with various instruments or equipment of different heights symmetrically installed. An anemometer is fixed in the northeast of the hollow-layer; it is 81 cm over the top of the largest equipment box, and 182 cm over the inclined plane in the model. However, the influence on the measured wind speed resulting from the two pillars symmetrically along the axis of 45° at the corners and the equipment installed on the hollow-out floor must be considered. The height of the anemometer at the hollow-layer is close to the gradient wind height, and the measured wind speed is slightly affected by the roughness of the surface roughness. However, the influence of the building, especially the symmetrical giant pillars along the 45 °axis and a large number of instrument boxes installed in the hollow-layer plane, and the measured wind speed must be considered.
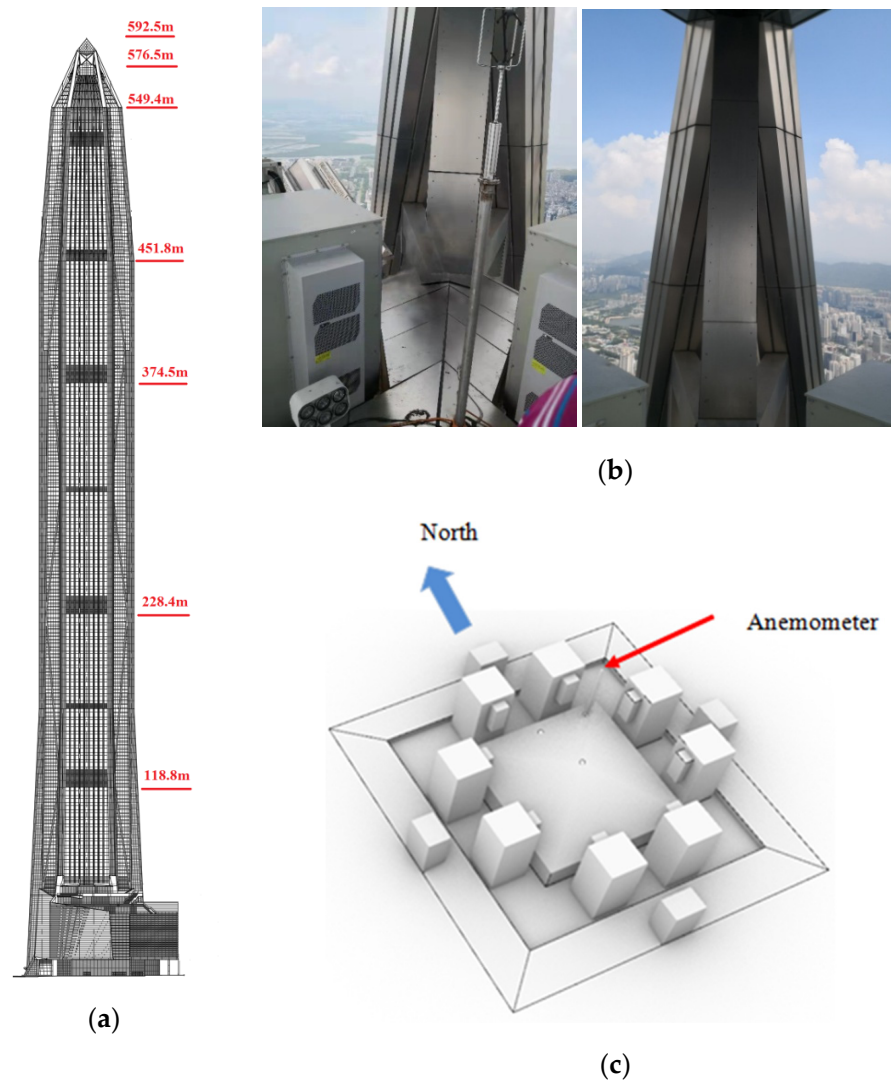
Figure 2. Information of PAFC: (**a**) building elevations; (**b**) position of anemometer and corner pillars; (**c**) details of the hollow-layer plane.

Super Typhoon Mangkhut (No. 1822) is one of the most disastrous tropical cyclones that landed on the coastal areas of South China in the recent 10 years, with the maximum wind level of 17 at the center during landfall [18,19]. The NLDI and PAFC sites completely recorded the wind speed from 0:00 to 24:00 (UTC + 8) on September 16, 2018 during the passage. Figure 3 shows the 10 min mean wind speed and wind direction curve. The NLDI station recorded the maximum mean wind speed of 40.7 m/s with the wind direction of 52° at 12:43, and the second maximum mean wind speed was 39.1 m/s with the wind direction of 84° at 14:47, indicating a slight difference between the results. Meanwhile, the maximum mean wind speed of 33.7 m/s at the PFAC site was recorded at 14:48 under the wind direction of 93°. Compared with tropical cyclones of super typhoon level, the wind speed record at an altitude of nearly 600 m was extremely small. This finding indicated the strong interference around the measured PAFC site. The dominant direction of strong wind in Shenzhen is east wind and its vicinity; thus, the wind directions of 84° for NLDI and 93° for PAFC are considered the maximum mean wind speeds when determining the reference wind pressure.

(a)

(b)
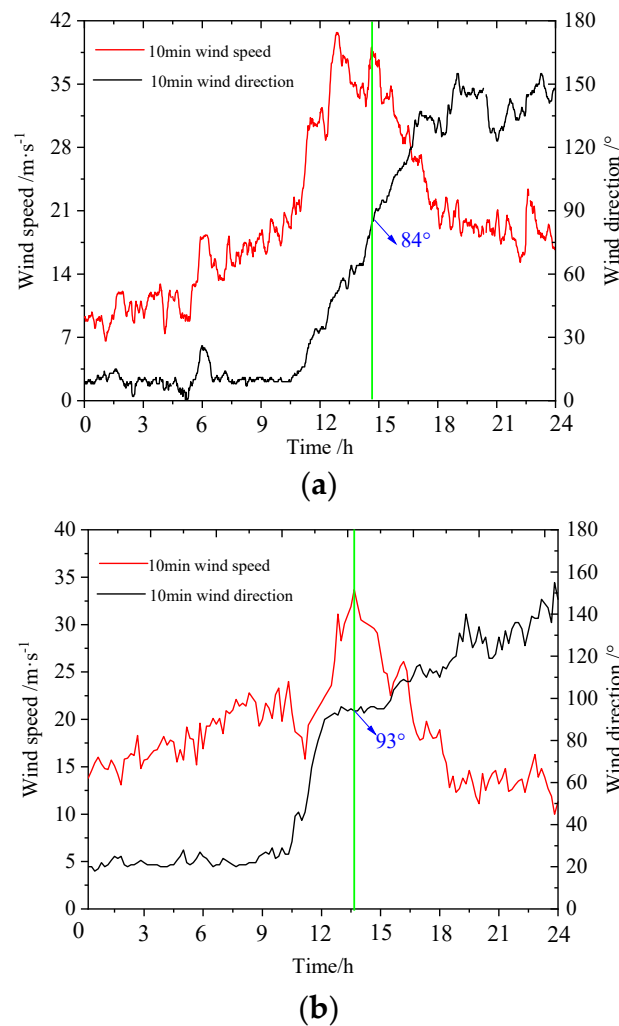
Figure 3. Observations of wind speed and direction at the sites of NLDI and PAFC during Typhoon Manghut: (**a**) NLDI; (**b**) PAFC.

3. Wind Speed Revise

3.1. NLDI Site

For NLDI, WTT was conducted to analyze the effect of the island itself on the wind speed collected by the anemometer, and numerical simulation was carried out for verification.

3.1.1. WTT

The WTT was carried out in the Wind Tunnel Laboratory of South China University of Technology, and a uniform air flow wind field was used. The maximum span of NLDI is approximately 4 km, and the maximum altitude is approximately 300 m. The scale ratio of the island model in the test is 1:1000, and the maximum blockage ratio of the model in the tunnel is 3.7%, thereby satisfying the test requirements. Figure 4a shows the test model located in the wind tunnel. Two Cobra probes were installed at the same height; one was at the anemometer position of the site, and the other was outside the upstream turntable away from the model (marked as the reference point). Both probes were set 65 mm over the floor, corresponding to the anemometer elevation of 65 m in the prototype. Two probes were always parallel to the axis of the wind tunnel as the turntable rotated to change the wind direction during the entire test. The sampling frequency of the probe was 400 Hz and the sampling time was 102.4 s during the experiment, as well as the accuracy of wind speed was usually ±0.5 m/s.
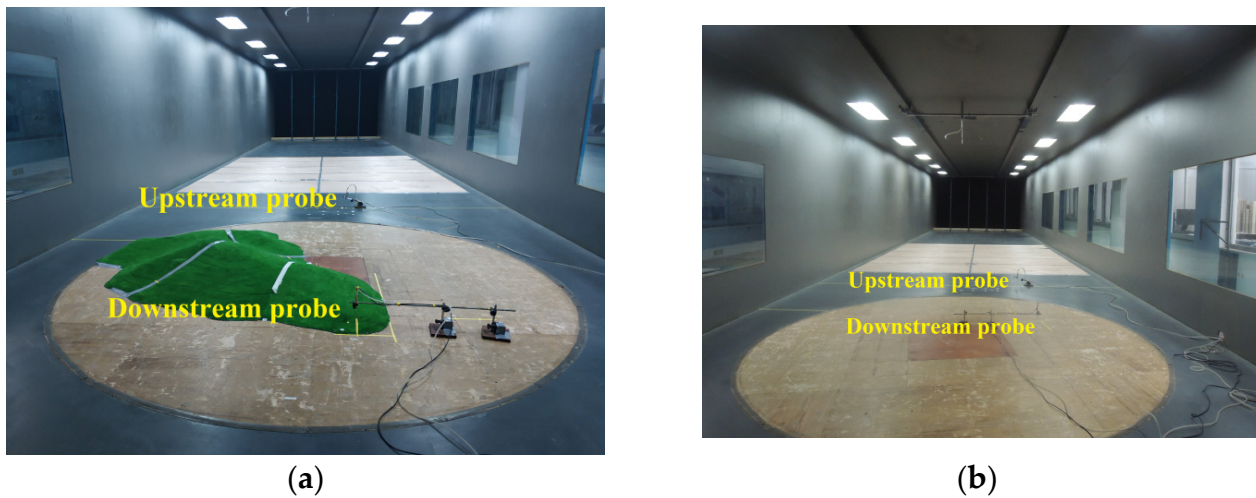
Figure 4. WTT model of Noi Ling Ding Island: (**a**) with NLDI; (**b**) without NLDI.

With regard to the impact of typhoon and geographical characteristics, WTT was only conducted for wind directions ranging from 0°–180°. Meanwhile, wind speeds of the upstream and downstream probes were compared without the island (Figure 4b). The figure shows that the wind speed of the downstream probe is 10% lower than that of the upstream in the empty wind tunnel mainly due to the shielding of the magnetic base that fixed the upstream probe. In view of the influencing factor, the wind speed at the downstream measured point would be revised.

3.1.2. Numerical Simulation Verification

ANSYS 16.0 was used in the numerical simulation of NLDI, which combined ICEM and Fluent software for pretreatment and calculation, respectively. The whole process followed these steps: (1) modeling of the actual terrain, (2) setting of computational domain, (3) division of computational grid, (4) definition of boundary conditions.

Modeling the surface with the traditional triangular mesh is relatively complicated due to the continuous fluctuation of the actual terrain. Therefore, the RhinoResurf plug-in based on Non-Uniform Rational B-Spline (NURBS) was used for landform surface reconstruction to improve the efficiency and accuracy. The Digital Elevation Model (DEM) data of NLDI were derived from Google Earth and transformed into a contour plot in CAD format; the contour lines should be continuous, closed, and disjointed. Then, the command item "create single NURBS surface from curve group" in the plug-in was selected to obtain the best fitting surface by adjusting the control parameters.

Considering different wind incident directions, the computational domain was set as an interior cylinder and an exterior cuboid; hence, wind directions were changed by rotating the interior domain. The distance from the inlet, outlet, and side wall of the computational domain to the island's edges should be sufficiently long to fully develop the turbulence in the 3D flow field [20,21] (Cheng W.C. and Liu C.H. 2011; Huang W.C. and Zhang X. 2019). The maximum altitude of the island marked as H was 0.3 km; thus, the dimensions of the exterior domain were $25 \times 8.2 \times 2.1$ km^3 (length $\times$ width $\times$ height). The inlet, side walls, and outlet were set to 2.1, 2.8, and 20 km away from the corresponding island's edge separately (Figure 5).
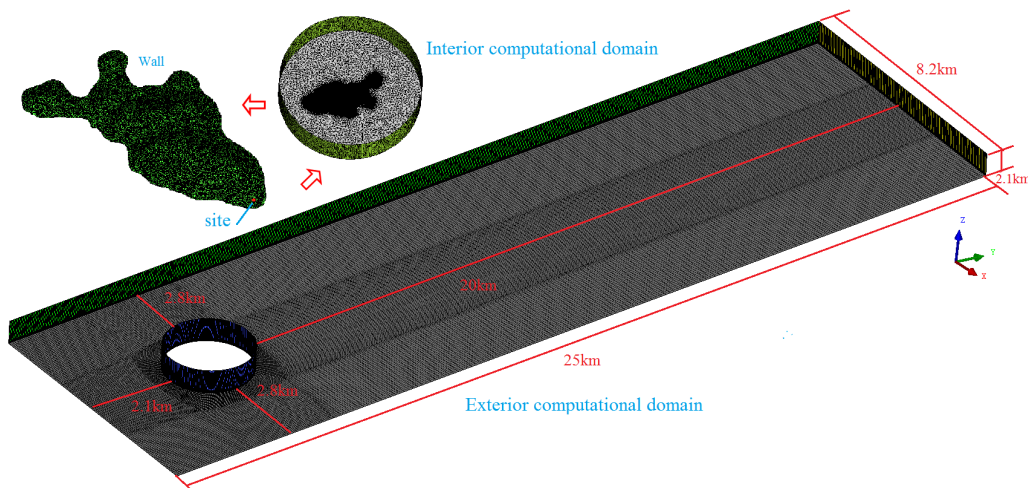
Figure 5. Computational domains and grids.

Hybrid grids were adopted in the mesh division, unstructured grids were used in the interior domain, and structured grids were used in the exterior domain. The interface operation was applied to connect these meshes. The near-wall grids should be refined, and the grid height y^+ of the first layer should be less than 5, owing to the enormous velocity gradient over the mountain surface. After several adjustments, the final mesh scheme was determined as follows: for unstructured grids in the inner domain, the grid height was 0.5 m in the first layer on the mountain surface, the maximum grid size was 20 m, the grid stretching ratio was 1.1, and the number of grid layers in the boundary layer was 15. For structural grids in the exterior domain, the minimum grid size in the horizontal direction was 50 m, and the maximal grid size was 200 m with a stretching ratio of 1.2. In the vertical direction, the size of the near-wall grid was 0.5 m, and the top grid size was 50 m with a stretching ratio of 1.1. The total number of grids in the computational domain was nearly 6 million.

The shear-stress transport k-ω (SST k-ω) model was selected as the turbulence model for simulations [21,22]. The model has good performance for the bounded wall and low Reynolds number flows, especially for the flow around. The boundary conditions were determined as follows: the vertical profile of the mean wind was used as the inlet boundary condition, and zero static pressure was applied at the outlet plane. The ground boundary is modeled as a rough wall with the roughness height of 0.00125 m and roughness constant of 0.75. The upper face and the lateral sides of the computational domain is modeled with symmetry boundary conditions. According to Yang Y. et al. [23] (2017), the SST k-ω model with the exponential mean velocity profile, turbulent kinetic energy, and its dissipation rate in numerical simulation are given by the following:

$$u_z = \frac{u_*}{k} \ln\left(\frac{z + z_0 * l_s}{z_0 * l_s}\right) \tag{1}$$

$$k = \frac{u_*^2}{\sqrt{C_\mu}} \sqrt{C_1 \ln\left(\frac{z + z_0 * l_s}{z_0 * l_s}\right) + C_2} \tag{2}$$

$$\omega = \frac{u_*}{k\sqrt{C_\mu}} \frac{1}{z + z_0 * l_s} \tag{3}$$

where z is the height from the ground, and U_z is the mean velocity at the height of z. u_* is the friction velocity with the value of 0.6 m/s. C_μ is the turbulence model constant given as 0.028. The two constants C_1 and C_2 are -0.36 and 5, respectively. z_0 is the aerodynamic ground roughness length related to terrain types, κ is the von Karman constant of 0.42, and the scale ratio l_s is 0.001. All the boundary conditions were defined through the user-defined functions provided by the fluent.

The computational settings include the pressure-based steady-state solver, the Semi-Implicit Method Pressure-Linked Equations (SIMPLEC) algorithm for the pressure–velocity coupling, and the second-order upwind format for the diffusion terms in the momentum and turbulence model equations. The convergence criteria of the scaled residuals for all the variables and the continuity equation are set to 10^{-5}. The relaxation factors of pressure, momentum and turbulent kinetic energy are 0.3, 0.7 and 0.8, respectively.

3.1.3. Experimental Results

The dominant wind direction of the Pearl River delta region is southeast wind to northeast wind. Therefore, the wind revision in incident directions ranging from $0°$ to $180°$ ($0°$ due north; clockwise rotation is positive) is sufficient to satisfy the revised requirements for gales in all typhoon measurements. The wind speeds at the NLDI site, the upstream reference point at the same height, and the wind speed influence coefficient (C_{VI}) are illustrated in Figure 6. The figure shows that the C_{VI} derived from the WTT and the CFD are consistent in the overall variation trend, but the former results are greater than the latter ones, quantitatively.
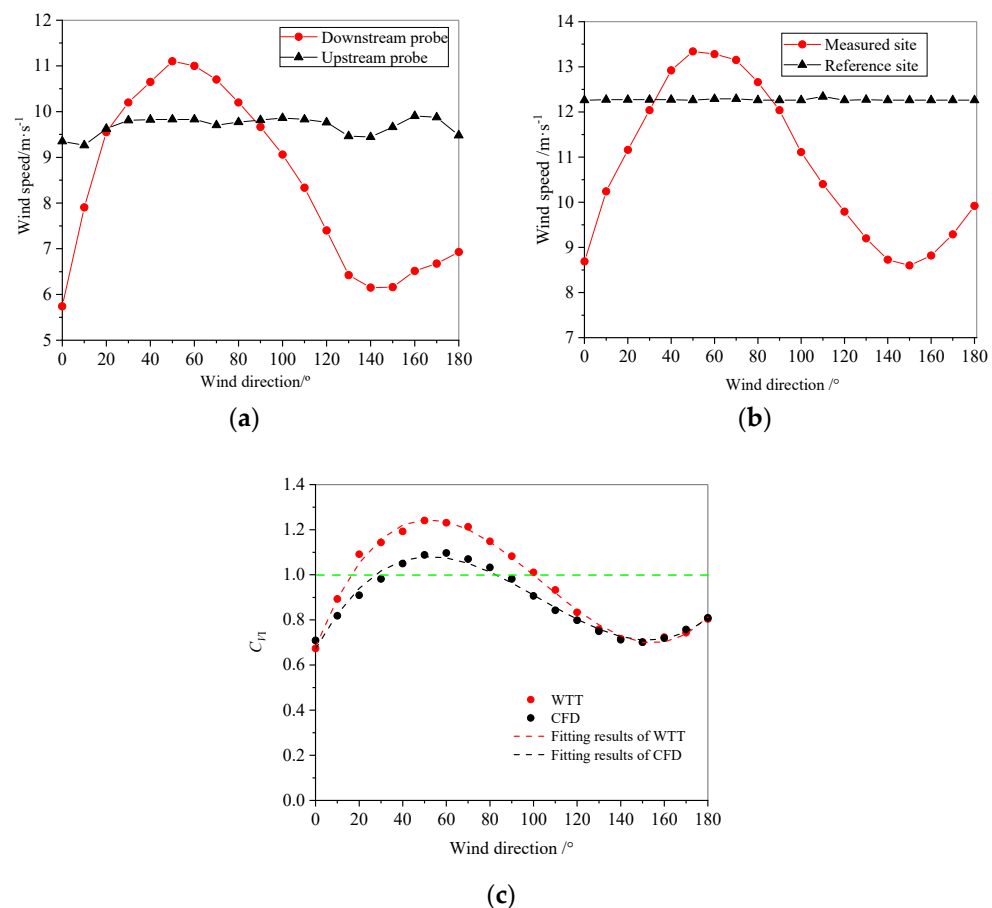
Figure 6. Description of experimental results: (**a**) relationship between wind speed and wind direction of WTT; (**b**) relationship between wind speed and wind direction of CFD; (**c**) variation of C_{VI} with wind direction of NLDI.

The WTT results revealed that the measured wind speeds were increased in different degrees due to the existence of the island under wind directions from $20°$ to $100°$. However, it decreased under the other wind directions. For the CFD simulated results, the wind directions that corresponded to the increased wind speeds were $30°$ to $90°$. Apparently, the WTT results were more sensitive due to the complex flow patterns, such as backflow and

reattachment in valleys and depressions, which can be reproduced in the WTT but difficult to simulate in CFD.

The least square method was implemented to fit the functional relationship between C_{VI} and wind directions by WTT and CFD. It provided guidance on correction when using the meteorological data collected at NLDI in the follow-up work. The polynomial fitting results of C_{VI} were provided as follows:

$$\begin{cases} C_{VI-\text{WTT}} = 0.000001008x^3 - 0.0003129x^2 + 0.02439x + 0.6809 & (R^2 = 0.9943) \\ C_{VI-\text{CFD}} = 0.0000007333x^3 - 0.0002258x^2 + 0.01763x + 0.6818 & (R^2 = 0.9833) \end{cases} \tag{4}$$

According to the measured wind speed of NLDI (Figure 3), the second maximum mean wind speed of 39.1 m/s under the wind direction 84° with the time of 14:47 should be revised. The C_{VI} corresponding to WTT is 1.12, and the C_{VI} corresponding to the numerical simulation is 1.00 according to Equation (4). Affected by the terrain, a slight acceleration effect was observed at the site under the sensitive wind direction, and the corrected wind speeds were less than or equal to the on-site measured ones. The correction effect of WTT on the measured wind speed was more significant.

3.2. PAFC Site

The wind measured site in the hollow-layer atop PAFC is greatly important to explain the high-altitude wind field in urban areas. However, the measured wind speeds are relatively inaccurate due to the blockage of the structural pillars at the corners and numerous installed equipment. WTTs were carried out with a segmental scale model of PAFC to explore the influence of relevant factors and to study the wind speed revise when considering the influence of architectural shape and surrounding environment.

The WTT was carried out in the Wind Tunnel Laboratory of South China University of Technology under the wind field of terrain category C. The segmental model of PAFC had an interception range from the tower top to 100 m below it, with a scale ratio of 1:100. The equipment was reduced to smaller scale and made by 3D printing. The maximum blockage ratio of the PAFC model in the tunnel was 3.52% and less than 5%, which satisfied the test requirement.

Two Cobra probes were fixed in the wind tunnel at these positions to reflect the relationship between the wind speed of the anemometer at the site and the upstream reference point with the same height, as shown in Figure 7. The upstream reference point was located at the edge of the turntable. When the model was installed, the anemometer atop the downstream tower should be located at the center of the turntable as far as possible. Meanwhile, the upstream Cobra probe was fixed on an automatically controlled abutment and was always maintained at the anemometer point by computer controlling.
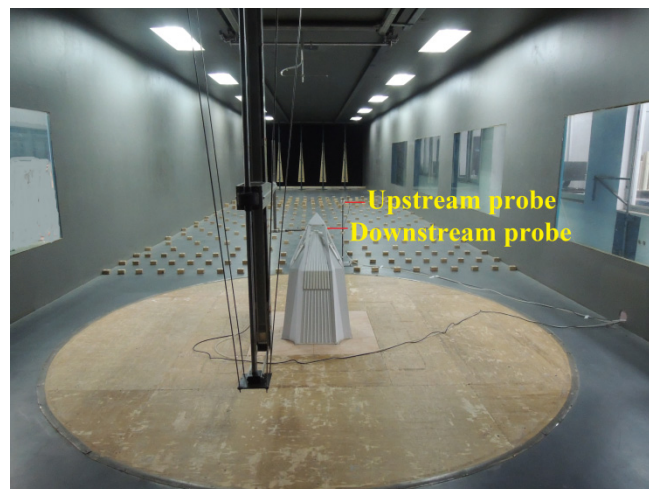

Figure 7. Overview of WTT.

During the test, the different wind incident directions were simulated by rotating the wind tunnel turntable, and the wind speeds of the probes were measured every 10° from 0° to 180° (restricted by test conditions and large structural pillars, 130° and 140° wind directions cannot be completed). Case 1 with instrument absence and case 2 with instrument presence were conducted to investigate the influence of instruments in the hollow-layer, as shown in Figure 8.

(**a**)   (**b**)
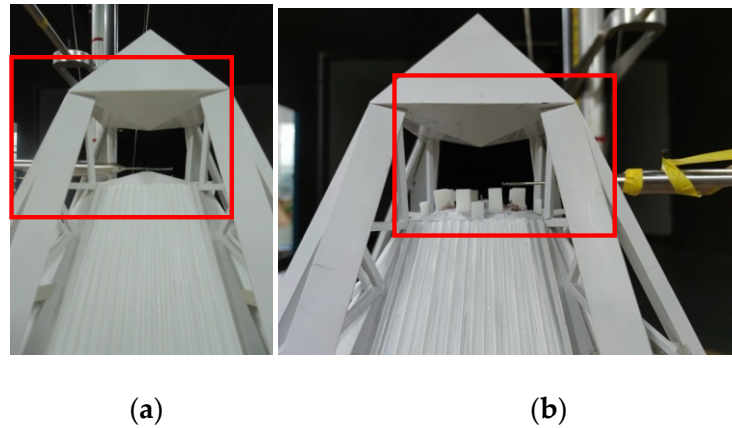
Figure 8. Details of the hollow-layer plane: (**a**) case 1 with instrument absence; (**b**) case 2 with instrument presence.

Figure 9 illustrates the variations of wind speed of the two probes with wind directions in two cases. The wind speed of the downstream probe was significantly decreased under the wind direction of 45° and nearby while increased in other directions in case 1, indicating that an acceleration effect similar to pipe ventilation is found in the hollow-layer without instruments. In case 2, the wind speeds of the downstream probe were less than those of the upstream probe in different degrees except for a few wind directions, owing to the shielding effect of the instruments. Wind speeds at the measured point of the scaled model were significantly smaller than those of the reference point in approximately 100° directions.

(**a**)   (**b**)
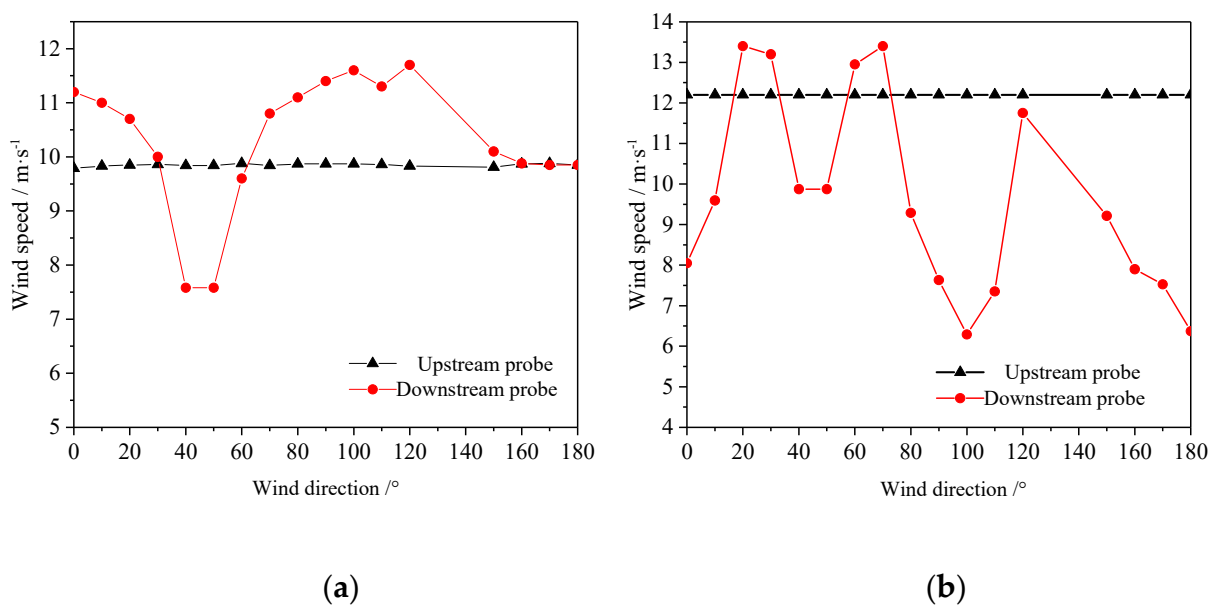
Figure 9. Variations of the wind speed with wind direction at the measured point of the segmental model of PAFC: (**a**) wind regime of case 1; (**b**) wind regime of case 2.

The variation of C_{VI} with wind direction in case 1 and case 2 is shown in Figure 10. The figure shows that, regardless of whether or not instruments exist, the C_{VI} is relatively close and changes symmetrically with 45° as the center, due to the geometric symmetry of the architectural scheme and the arrangement of instruments, within the wind direction range of 45° ± 25°. According to the C_{VI} at these directions, the wind speed reduction of the corresponding wind incident direction is as high as 20% due to the corner giant pillars designed for architectural requirements. In addition, the instruments greatly affected the wind speed, especially under the wind direction of 90° or nearby; a serious shielding effect of instruments was observed. The C_{VI} was 0.625 under the wind direction of 90° and 0.515 under the wind direction of 100°. The experimental results verify that the measured wind speed atop PAFC was far less than the wind incident direction at the same height. The maximum 10 min mean wind speed atop PAFC was 33.7 m/s during Super Typhoon Mangkhut, which occurred in the wind direction of 93°. According to the WTT results, the measured wind speed was seriously underestimated. Therefore, the corrected wind speed was approximately 56.9 m/s by linear interpolation.
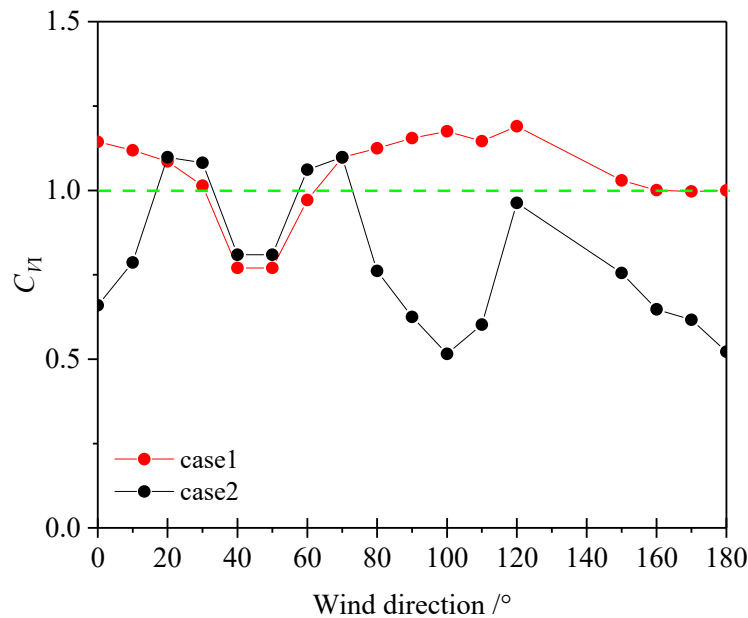

Figure 10. Variation of CVI with wind direction of PFAC.

4. Maximum Reference Wind Pressure of Super Typhoon Mangkhut

The basic wind pressure defined in the Load Code for the Design of Building Structures in China [24] is as follows: the mean 10 min maximum wind speed obtained by statistics in 50 years at the height of 10 m above the ground on the relatively open landform is the maximum basic wind speed, and the wind basic pressure is equal to 1/1600 of the square of the maximum basic wind speed. Then, the values of the actual reference wind pressure in Shenzhen during Super Typhoon Mangkhut are discussed according to the C_{VI} of these sites.

Vickery et al. [25] (2009) proposed a typhoon boundary layer model applicable to the sea based on the measured results of the downcast anemometer and the theoretical typhoon boundary layer model of Kerpert [26]. The model could be expressed as follows:

$$\begin{cases} U(z) = \frac{u_*}{\kappa}\left[\ln\left(\frac{z}{z_o}\right) - 0.4\left(\frac{z}{H^*}\right)^2\right] \\ H^* = 343.7 + 0.260/I \\ I = \sqrt{\left(f + \frac{2V}{r}\right)\left(f + \frac{V}{r} + \frac{\partial V}{\partial r}\right)} \\ H = 1.12 \times H^* \end{cases} \tag{5}$$

where V is the tangential mean gradient wind speed, which can be ignored in calculation. H^* is the boundary layer height parameter, which is inversely proportional to the inertia stability I, and the value ranges from 300 m to 1200 m based on Vickery's measured data. H is the boundary layer thickness, κ is the von Karman coefficient with a value of 0.4, and u_* is friction velocity. z_0 is the aerodynamic rough length, which is equal to 0.002 m in an open water area and 0.2 m in flat landform of dense urban suburb [27]. f is the Coriolis force coefficient.

Assuming that the boundary layer thickness is 1000 m, then the wind speed of NDLI at 65 m height is revised as 34.9 m/s under the direction of 84° according to the WTT results. Hence, the maximum 10 min mean wind speed at 10 m height of the station is deduced as 29.01 m/s based on the profile formula. The value of 29.01 m/s can be approximately considered the maximum 10 min mean wind speed at 10 m height in Shenzhen during the typhoon because NLDI is very close to urban areas. Consequently, the converted reference pressure is 0.526 kPa. The 576 m height wind speed of PAFC at a wind direction of 93° is corrected as 56.9 m/s according to the WTT results, and it can be regarded as the gradient wind speed in this area. The maximum 10 min mean wind speed at 10 m height is deduced as 28.42 m/s. Thus, the converted reference pressure is 0.505 kPa. The reference wind pressures converted from the measured wind speeds of the typhoon at the two sites are relatively close to each other. The results are higher than the basic wind pressure of 0.45 kPa in the 10-year return period stipulated in the Load Code for the Design of Building Structures of China [24] but lower than that of 0.75 kPa in the 50-year return period.

5. Conclusions

We discussed the deviation revision of the measured meteorological data caused by the impact of the local wind environment and the accurate value of reference wind pressure in Shenzhen during Super Typhoon Mangkhut. Relevant studies on the two sites of NLDI and PAFC were carried out by WTT and CFD numerical simulation methods. The conclusions are summarized as follows:

1. As for NLDI, which was affected by terrain interference, the overall trend of the fitted C_{VI} with wind direction by means of WTT and numerical simulation is the same. However, differences in C_{VI} were found under the same wind direction, and the C_{VI} value in the WTT was higher than that in the CFD numerical simulation. The existence of NLDI accelerated the measured wind speed by 12% in the sensitive wind direction.
2. As for PAFC, which was affected by the building and instruments, the WTT results revealed that the wind speed in directions of 45° and nearby were sheltered by the giant pillars at the corner and reduced by 20%. The wind speeds of the other wind directions were mainly affected by the instruments in the hollow-layer, and the acceleration effect was presented when the instruments were absent. In addition, the shielding effect was presented when the instruments were present. In the dominant wind direction, the wind speed influence coefficients were 1.163 and 0.593 when undisturbed and disturbed by instruments.
3. The C_{VI} results were used to correct the recorded wind speed at the NLDI and PAFC sites during Super Typhoon Manghut; they were converted into the 10 min mean wind pressure value at 10 m height under the standard landform. Hence, the reference wind pressure values calculated were 0.526 and 0.505 kPa. The analogous conversion values achieved the purpose of mutual verification. Meanwhile, the effectiveness and reliability of the methodologies are presented.

Author Contributions: Conceptualization, J.D. and Z.X.; methodology, J.D.; formal analysis, X.C.; writing—original draft preparation, J.D.; writing—review and editing, Z.X. and L.Z.; supervision, J.D., Z.X. and L.Z. All authors have read and agreed to the published version of the manuscript.

Institutional Review Board Statement: Not applicable.

Informed Consent Statement: Not applicable.

Data Availability Statement: All data included in this study are available upon request by contact with the corresponding author.

Conflicts of Interest: The authors declare no conflict of interest.

References

1. Wang, F.; Chen, X.; He, R.; Liu, Y.; Hao, J.; Li, J. Wind Characteristics in Mountainous Valleys Obtained through Field Measurement. *Appl. Sci.* **2021**, *11*, 7717. [CrossRef]
2. Wang, J.; Li, J.; Wang, F.; Hong, G.; Xing, S. Research on Wind Field Characteristics Measured by Lidar in a U-Shaped Valley at a Bridge Site. *Appl. Sci.* **2021**, *11*, 9645. [CrossRef]
3. Teunissen, H.; Shokr, M.; Bowen, A.; Wood, C.; Green, D. The Askervein Hill Project: Wind-tunnel simulations at three length scales. *Bound.-Layer Meteorol.* **1987**, *40*, 1–29. [CrossRef]
4. Raithby, G.; Stubley, G.; Taylor, P.A. The Askervein hill project: A finite control volume prediction of three-dimensional flows over the hill. *Bound.-Layer Meteorol.* **1987**, *39*, 247–267. [CrossRef]
5. Castro, F.; Palma, J.; Lopes, A. Simulation of the Askervein flow. Part 1: Reynolds averaged Navier-Stokes equations (*k-ε* turbulence model). *Bound.-Layer Meteorol.* 2003; 107, 501–530.
6. Silva Lopes, A.; Palma, J.; Castro, F. Simulation of the Askervein flow. Part 2: Large-eddy simulations. *Bound.-Layer Meteorol.* **2007**, *125*, 85–108. [CrossRef]
7. Moreira, G.; Dos Santos, A.; Do Nascimento, C.; Valle, R. Numerical study of the neutral atmospheric boundary layer over complex terrain. *Bound.-Layer Meteorol.* **2012**, *143*, 393–407. [CrossRef]
8. Flay, R.; King, A.; Revell, M.; Garpenter, P.; Turner, R. Wind speed measurements and predictions over Belmont Hill, Wellington, New Zealand. *J. Wind. Eng. Ind. Aerodyn.* **2019**, *195*, 104018. [CrossRef]
9. *AS/NZS1170.2.2011 Australia/New Zealand Standard, Structural Design Actions. Part 2: Wind Actions*; Standards Australia International Ltd.: Sydney, Australia; Standards New Zealand: Wellington, New Zealand, 2011.
10. Zhang, W.; Liu, M.; Wang, K.; Zhang, F.; Hou, L. Numerical Study on the Gas Leakage and Dispersion at the Street Intersection of a Building Group. *Comput. Modeling Eng. Sci.* **2020**, *123*, 1247–1266. [CrossRef]
11. Janssen, W.; Blocken, B.; van Hooff, T. Pedestrian wind comfort around buildings: Comparison of wind comfort criteria based on whole-flow field data for a complex case study. *Build. Environ.* **2013**, *59*, 547–562. [CrossRef]
12. Blocken, B.; Stathopoulos, T.; van Beeck, J. Pedestrian-level wind conditions around buildings: Review of wind-tunnel and CFD techniques and their accuracy for wind comfort assessment. *Build. Environ.* **2016**, *100*, 50–81. [CrossRef]
13. Li, B.; Luo, Z.; Sandberg, M.; Liu, J. Revisiting the 'Venturi effect' in passage ventilation between two non-parallel buildings. *Build. Environ.* **2015**, *94*, 714–722. [CrossRef]
14. Iqbal, Q.; Chan, A. Pedestrian level wind environment assessment around group of high-rise cross-shaped buildings: Effect of building shape, separation and orientation. *Build. Environ.* **2016**, *101*, 45–63. [CrossRef] [PubMed]
15. Jamińska-Gadomska, P.; Lipecki, T.; Pieńko, M.; Podgórski, J. Wind velocity changes along the passage between two angled walls—CFD simulations and full-scale measurements. *Build. Environ.* **2019**, *157*, 391–401. [CrossRef]
16. James Lo, L.; Banks, D.; Novoselac, A. Combined wind tunnel and CFD analysis for indoor airflow prediction of wind-driven cross ventilation. *Build. Environ.* **2013**, *60*, 12–23. [CrossRef]
17. Ramponi, R.; Blocken, B. CFD simulation of cross-ventilation for a generic isolated building: Impact of computational parameters. *Build. Environ.* **2012**, *53*, 34–48. [CrossRef]
18. Zhang, L.L.; Hu, X.Q.; Xie, Z.N.; Shi, B.Q.; Zhang, L.; Wang, R.H. Field measurement study on time-varying characteristics of modal parameters of super high-rise buildings during super typhoon. *J. Wind. Eng. Ind. Aerodyn.* **2020**, *200*, 104139. [CrossRef]
19. Zhou, K.; Li, Q.S.; Li, X. Dynamic Behavior of Supertall Building with Active Control System during Super Typhoon Mangkhut. *J. Struct. Eng.* **2020**, *146*, 04020077. [CrossRef]
20. Cheng, W.; Liu, C. Large-eddy simulation of turbulent transports in urban street canyons in different thermal stabilities. *J. Wind. Eng. Ind. Aerodyn.* **2011**, *99*, 434–442. [CrossRef]
21. Huang, W.; Zhang, X. Wind field simulation over complex terrain under different inflow wind directions. *Wind. Struct.* **2019**, *28*, 239–253.
22. Argyropoulos, C.D.; Markatos, N.C. Recent advances on the numerical modelling of turbulent flows. *Appl. Math. Model.* **2015**, *39*, 693–732. [CrossRef]
23. Yang, Y.; Xie, Z.N.; Gu, M. Consistent inflow boundary conditions for modelling the neutral equilibrium atmospheric boundary layer for the SST k-ω model. *Wind. Struct.* **2017**, *24*, 465–480. [CrossRef]
24. *Load Code for the Design of Building Structures, GB 5009-2012*; Ministry of Construction: Beijing, China, 2012.
25. Vickery, P.; Wadhera, D.; Powell, M.; Chen, Y. A Hurricane boundary layer and wind field model for use in engineering applications. *Appl. Meteorol. Climatol.* **2009**, *48*, 381–405. [CrossRef]

26. Kepert, J. The dynamics of boundary layer jets within the tropical cyclone core. Part I: Linear theory. *J. Atmos. Sci.* **2001**, *58*, 2469–2484. [CrossRef]

27. He, J.Y.; Li, Q.S.; Chan, P.W.; Li, L.; Lu, C.; Zhang, L.; Yang, H.L. Characteristics and Vertical Profiles of Mean Wind and Turbulence for typhoon, Monsoon, and Thunderstorm Winds. *J. Struct. Eng.* **2021**, *147*, 04021188. [CrossRef]